Mineralogy and Petrology (2023) 117:269–280
https://doi.org/10.1007/s00710-023-00830-5

RESEARCH

Prachařite, $CaSb^{5+}_2(As^{3+}_2O_5)_2O_2{\cdot}10H_2O$, a new mineral from Lavrion, Greece

Uwe Kolitsch[1,2] · Jiří Sejkora[3] · Dan Topa[1] · Anthony R. Kampf[4] · Jakub Plášil[5] · Branko Rieck[2] · Karl Heinz Fabritz[6]

Received: 31 October 2022 / Accepted: 18 April 2023 / Published online: 9 June 2023
© The Author(s) 2023

Abstract

Prachařite, ideally $CaSb^{5+}_2(As^{3+}_2O_5)_2O_2{\cdot}10H_2O$, is a new mineral found in underground workings of the Plaka Mine No. 80, Plaka, Lavrion Mining District, Attica, Greece. It occurs as colourless to white, thin tabular hexagonal, in general sharp crystals up to 2.5 mm in diameter, and is associated with pharmacolite, sulphur and very rare smamite $\{Ca_2Sb(OH)_4[H(AsO_4)_2]{\cdot}6H_2O\}$ on a matrix composed of sphalerite, galena and carbonate gangue. Prachařite is translucent to transparent, with a glassy lustre, white streak, a good cleavage parallel to {0001} and a distinct cleavage parallel to $\{10\bar{1}0\}$. It is non-luminescent, brittle, and has an uneven fracture, a Mohs hardness of 2–2.5 and X-ray density $D_x = 2.848$ g/cm^3, $D_{calc.} = 2.836$–2.853 g/cm^3 (for two measured compositions). Optically, it is uniaxial negative, with $\omega = 1.619(1)$ and $\varepsilon = 1.553(1)$. Prachařite is trigonal, space group $P\bar{3}c1$ (no. 165), with $a = 13.951(2)$, $c = 19.899(2)$ Å, $V = 3354.1(10)$ Å^3 and $Z = 6$. Strongest lines in the X-ray powder diffraction pattern are [d in Å (I) hkl]: 9.894 (100) 002; 6.045 (8) 200; 5.156 (10) 202; 4.946 (11) 004; 3.297 (19) 311, 006, 222; 2.988 (22) 400, 313, 116. Two sets of independent electron probe micro-analyses yielded (wt%): CaO 6.28/7.12, MgO 0.09/-, Zn -/0.01, Sb_2O_5 39.22/40.19, As_2O_3 47.59/47.39, SO_3 -/0.02, H_2O 21.65/22.04 (calculated on the basis of ideal composition derived from crystal-structure determination), total 114.83/116.77; the total is reproducibly high due to a loss of a third of all water molecules under the electron beam. The empirical formulae, based on O = 22 atoms per formula unit, for the two datasets are very similar, $(Ca_{0.93}Mg_{0.02})_{\Sigma 0.95}Sb_{2.02}(AsO_3)_{4.00}{\cdot}10H_2O$ and $Ca_{1.04}Sb_{2.03}(AsO_3)_{3.92}{\cdot}10H_2O$. The ideal formula is $CaSb^{5+}_2(As^{3+}_2O_5)_2O_2{\cdot}10H_2O$, determined with the help of a crystal-structure determination based on single-crystal X-ray diffraction datasets collected at room temperature ($R1 = 2.3\%$). The atomic arrangement of prachařite is unusual; it is based on two different layers containing a six-membered ring of corner-sharing SbO_6 octahedra, an eight-coordinated Ca1 atom in the centre of the ring, two non-equivalent AsO_3 groups corner-linked to form a $(As_2O_5)^{4-}$ diarsenite group, and, on interlayer sites, a seven-coordination Ca2 atom and three water molecules (all only weakly hydrogen-bonded), one of which is only partially occupied (split position). The mineral is named in honour of Dr Ivan Prachař, a long-term researcher of the mineralogy and underground workings of Lavrion.

Keywords Prachařite · New mineral · Crystal structure · Plaka Mine No. 80 · Lavrion Mining District

Editorial handling: K. Friese

✉ Uwe Kolitsch
uwe.kolitsch@nhm-wien.ac.at

[1] Mineralogisch-Petrographische Abteilung, Naturhistorisches Museum Wien, Burgring 7, A-1010 Wien, Austria

[2] Institut für Mineralogie und Kristallographie, Universität Wien, Josef-Holaubek-Platz 2, A-1090 Wien, Austria

[3] Department of Mineralogy and Petrology, National Museum, Cirkusová 1740, 193 00 Prague 9, Czech Republic

[4] Mineral Sciences Department, Natural History Museum of Los Angeles County, 900 Exposition Blvd., Los Angeles, CA 90007, USA

[5] Institute of Physics ASCR, v.v.i, Na Slovance 2, CZ-182 21 Prague 8, Czech Republic

[6] August-Novy-Str. 24, 3108 Sankt Pölten, Austria

Introduction

During some of the authors' (UK, BR, KHF) ongoing studies of the mineralogy and mines of the famous Lavrion mining district in Greece (Bonsall et al. 2011; Scheffer et al. 2019 and references therein), we encountered, in 2016, a colourless to white supergene mineral on weathered lead–zinc ore, whose thin tabular, six-sided crystal morphology did not remind us of any known species. In fact, a full characterisation of the mineral, including a determination of its crystal structure, showed that it is a new, unusual hydrated oxysalt species containing Ca, Sb(V) and As(III). The mineral and its name were subsequently approved by the International Mineralogical Association's Commission on New Minerals, Nomenclature and Classification (IMA 2018-081).

The mineral is named after Dr Ivan Prachař (b. 1957) of Prague, Czech Republic. Dr Prachař has, in close collaboration with one of the authors (KHF), studied the mineralogy of the numerous Lavrion mines for more than 20 years and helped to carefully survey and document all the underground workings (ancient to modern). Several discoveries of rare and unusual minerals in Lavrion are due to his work. The name is pronounced pra-haɟ-ait.

The present contribution provides a full characterisation of prachařite and a comparison with related species. Cotype material is deposited in the Natural History Museum, Vienna, Austria (one cotype specimen and the crystal used for the crystal-structure solution; catalogue no. NHMW-MIN-O357), in the National Museum, Prague, Czech Republic (one cotype specimen, catalogue no. P1P 15/2018), and in the Natural History Museum of Los Angeles County, USA (one cotype specimen, catalogue no. 67242).

Occurrence and paragenesis

Prachařite was found in September 2016 in underground workings of the Plaka Mine No. 80, Plaka, Lavrion Mining District, Lavreotiki, Attica, Greece. The Plaka Mine No. 80 is located in the northern part of the famous Lavrion mining district (Leleu 1966, 1969; Skarpelis 2007; Voudouris et al. 2008; Skarpelis and Argyraki 2009; Bonsall et al. 2011; Scheffer et al. 2019). This mine is known for late-stage hydrothermal As-Sb-Pb–Zn(-Ag) ore veins with assemblages of primary silver minerals and a large variety of supergene phases, mainly arsenates (Wendel and Markl 1996; Rieck and Rieck 1999; Rieck et al. 2018, 2020, 2022; Frenzel et al. 2022). About 133 mineral species are currently (May 2023) known from the mine.

On the collected material, prachařite is accompanied by pharmacolite, a few tiny sulphur crystals and very rare smamite $\{Ca_2Sb(OH)_4[H(AsO_4)_2]\cdot 6H_2O\}$ (the latter only as a unique crystal, adjacent to a prachařite crystal, on a single, very small specimen; Rieck et al. 2022). These supergene phases crystallised on an ore matrix composed of dark brownish sphalerite, galena and carbonate gangue (dolomite and calcite). The vein-type primary ore mineralisation at this locality is composed of sphalerite, galena, pyrite, arsenic, stibarsen, stibnite and other phases. Typical secondary minerals include pharmacolite, picropharmacolite (very common), various Ca arsenates [including the unnamed phase $Ca_5(AsO_4)_2(HAsO_4)_2\cdot 5H_2O$, Kolitsch et al. 2014], antimony oxides, sulphur and others.

Morphological, physical and optical properties

Prachařite forms colourless to white, thin tabular hexagonal, in general sharp crystals up to 2.5 mm in diameter, but mostly 1–1.5 mm (Figs. 1 and 2). Parts of the crystals may appear somewhat crumbly, with recognisable cleavage cracks. The colourless platelets may show a frosted tabular face and a very thin white opaque rim. Prachařite is translucent to transparent, with a glassy lustre, white streak, a good cleavage parallel to {0001} and a distinct cleavage parallel to $\{10\bar{1}0\}$. It is non-luminescent, brittle, and has an uneven fracture and a Mohs hardness of 2–2.5. Optically, it is uniaxial negative, with $\omega = 1.619(1)$ and $\varepsilon = 1.553(1)$ (determined in white light) and nonpleochroic. Mass density was not measured directly; the X-ray density D_x is 2.848 g/cm^3 (based on single-crystal data measured in Vienna—see below). For the ideal composition and the Vienna single-crystal data $D_{calc.} = 2.838$ g/cm^3; for the measured compositions (see following section), $D_{calc.} = 2.836$–2.853 g/cm^3.

Fig. 1 Colourless thin tabular hexagonal crystal of prachařite. Area on cotype specimen P1P 15/2018. White-light photomicrograph Jiří Sejkora

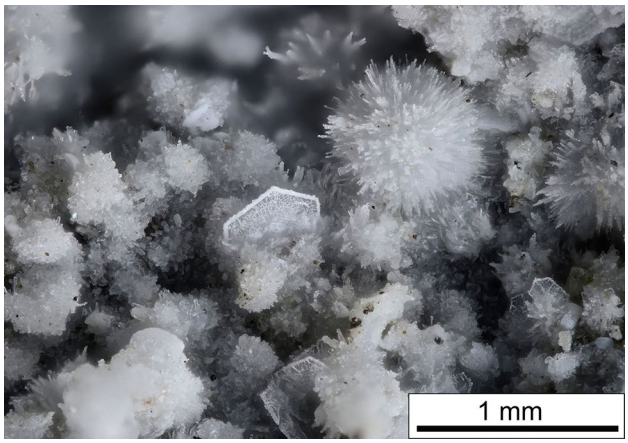

Fig. 2 Colourless thin tabular hexagonal crystal of prachařite associated with white sprays of indistinct acicular pharmacolite crystals. Area on co-type specimen NHMW-MIN-O357. White-light photomicrograph Harald Schillhammer

Chemical composition

Chemical analyses of prachařite were carried out with two electron probe micro-analysers, with very similar results for the standard polished mounts. The cotype material in Prague was quantitatively analysed with a Cameca SX 100 instrument (wavelength-dispersive mode, 15 kV, 4 nA, 10 µm defocussed beam diameter). Contents of Al, Bi, Cl, Co, Cu, Fe, K, Mn, Na, Ni, P, Pb, S, Si, V and Zn were all below detection limits. The following X-ray lines and reference materials were used: (i) *K*α lines: Ca (wollastonite), Mg (synthetic Mg_2SiO_4), *L*α line: As (lammerite); (ii) *L*β line: Sb (synthetic Sb). Counting times were 20 s on peak and 10 s on each background position. The raw intensities were converted to the concentrations automatically using the *PAP* (Pouchou and Pichoir 1985) matrix-correction software. The H_2O content could not be determined directly, because of the very meagre amount of pure material. The H_2O content was therefore calculated on the basis of 10 H_2O per formula unit (pfu) from the crystal-structure analysis. Results are given in Table 1. The high analytical totals after the addition of the calculated H_2O content (114.83) are caused by partial dehydration of the sample (about half of the total water content) under the vacuum conditions of the instrument chamber and due to visible beam damage; dehydration is reflected by abundant dehydration fractures in the crystal grains. We also tried to vary measurement conditions, using a beam current of up to 1 nA and a beam diameter of 20 µm, however, with the same results. Finally, we note that the observation of variable transparency of the crystals may indicate possible prior partial dehydration of those crystals that are translucent or not transparent. The material in Vienna was quantitatively analysed with a JEOL "Hyperprobe" JXA 8530F field-emission gun electron probe micro-analyser (EPMA),

Table 1 Results of EPMA chemical analyses of prachařite

Cotype material in Prague (no. of analyses: 8)			
Constituent	Mean	Range	SD
CaO	6.28	6.02–6.55	0.19
MgO	0.09	0.00–0.19	0.07
Sb_2O_5	39.22	38.10–40.26	0.59
As_2O_3	47.59	45.05–49.23	1.27
H_2O	21.65[a]		
Total	114.83		
Cotype material in Vienna (no. of analyses: 20)			
Constituent	Mean	Range	SD
CaO	7.12	6.82–7.43	0.15
ZnO	0.01[b]	0.00–0.07	0.02
Sb_2O_5	40.19	38.75–41.37	0.72
As_2O_3	47.39	46.33–48.73	0.75
SO_3	0.02[b]	0.00–0.07	0.02
H_2O	22.04[a]		
Total	116.77		

All values are quoted in wt%

SD standard deviation

[a]Content of H_2O was calculated on the basis of ideal composition (10 H_2O pfu) derived from the crystal-structure determination

[b]Detection limits (ppm) are: Zn 360, S 100; this may imply that the values for Zn and S are spurious. Mg was measured, but was clearly below the detection limit

Table 2 Powder X-ray diffraction data (*d* in Å) for prachařite

I_{obs}	d_{obs}	I_{obs}	d_{obs}	d_{calc}	I_{calc}	*hkl*	I_{obs}	d_{obs}	d_{calc}	I_{calc}	*hkl*
data 1		data 2					data 2				
3	12.089	16	12.15	12.0850	7	1 0 0			1.9031	1	5 1 5
100	**9.894**	**100**	**9.96**	9.8948	100	0 0 2			1.9007	1	3 3 6
5	7.655	21	7.68	7.6560	13	0 1 2			1.8807	1	2 0 10
4	6.980	17	6.92	6.9773	9	1 1 0			1.8569	2	2 5 3
				6.5803	2	1 1 1	13	1.8479	1.8385	6	3 1 9
8	**6.045**	**33**	**6.05**	6.0425	17	2 0 0			1.8350	1	1 6 1
6	5.703	24	5.73	5.7022	12	1 1 2			1.8131	1	1 5 6
10	**5.156**	**30**	**5.16**	5.1570	15	2 0 2			1.7385	1	5 2 5
11	**4.946**	10	4.96	4.9474	8	0 0 4			1.7264	2	5 3 0
1	4.794	5	4.77	4.7934	3	1 1 3			1.7213	1	2 2 10
				4.5786	1	0 1 4	**30**	**1.7170**	1.7199	6	3 5 1
4	4.451	15	4.45	4.4507	7	2 1 1			1.7041	1	3 1 10
1	3.443	2	3.862	3.8280	1	0 2 4			1.7007	3	5 3 2
				3.4887	1	2 2 0			1.6945	1	3 3 8
		3	3.435	3.4426	2	1 1 5			1.6888	2	4 1 9
2	3.352			3.3518	5	3 1 0			1.6759	1	6 2 0
7	3.305	**59**	**3.314**	3.3047	16	3 1 1			1.6702	2	3 5 3
19	**3.297**			3.2983	12	0 0 6	16	1.6677	1.6691	1	5 2 6
				3.2901	4	2 2 2			1.6554	1	4 0 10
		14	3.180	3.1819	2	1 0 6			1.6524	3	2 6 2
4	3.175			3.1746	7	3 1 2			1.6491	1	0 0 12
				3.0839	1	2 2 3			1.6315	1	5 1 8
				3.0213	2	4 0 0			1.6300	1	5 3 4
22	**2.988**	**95**	**2.994**	2.9882	48	3 1 3			1.5978	1	3 3 9
				2.9819	2	1 1 6			1.5969	1	2 5 7
2	2.896			2.8951	5	0 2 6			1.5955	1	1 7 1
4	2.890	22	2.881	2.8896	5	4 0 2	**26**	**1.5935**	1.5909	1	0 2 12
4	2.851			2.8511	6	2 2 4			1.5873	1	6 2 4
				2.6740	1	1 2 6			1.5852	7	3 1 11
1	2.637	12	2.633	2.6372	2	4 1 0			1.5824	3	5 3 5
				2.6202	1	1 1 7	3	1.5512	1.5556	1	1 7 3
2	2.615			2.6141	5	4 1 1			1.5296	1	3 5 6
2	2.579	**31**	**2.570**	2.5785	2	4 0 4	8	1.5297	1.5242	1	5 2 8

Table 2 (continued)

5	2.558			2.5578	12	1 3 5
				2.5559	1	3 2 3
				2.5482	1	4 1 2
8	2.4738	10	2.484	2.4737	9	0 0 8
				2.4487	2	4 1 3
		4	2.423	2.4170	1	5 0 0
				2.4039	1	1 2 7
1	2.3511			2.3509	3	1 3 6
		13	2.337	2.3315	1	1 1 8
1	2.3271			2.3272	3	4 1 4
				2.3258	1	3 3 0
				2.2893	1	0 2 8
				2.2688	1	4 2 1
				2.2641	1	3 3 2
				2.2279	1	4 0 6
				2.1946	1	1 4 5
		7	2.1762	2.1717	1	0 5 4
1	2.1702			2.1705	2	5 1 0
				2.1610	1	3 1 7
1	2.1581			2.1582	1	4 2 3
1	2.1204	2	2.1306	2.1201	2	5 1 2
2	2.0617	4	2.0650	2.0618	2	5 1 3
				2.0052	1	3 3 5
1	1.9908	13	1.9944	1.9903	3	3 1 8
1	1.9876			1.9877	3	5 1 4
1	1.9810			1.9790	2	0 0 10
				1.9479	1	4 3 2
1	1.9351			1.9352	3	5 2 0
		17	1.9286	1.9284	2	1 4 7
				1.9260	2	5 2 1
				1.9140	1	4 0 8
				1.4941	2	6 2 6
8	1.4933			1.4862	1	4 1 11
				1.4839	1	7 1 5
				1.4797	1	1 3 12
				1.4734	4	5 3 7
18	1.4729			1.4723	3	7 2 1
				1.4624	1	5 1 10
				1.4603	1	2 7 2
				1.4527	1	2 5 9
7	1.4470			1.4475	1	0 4 12
				1.4408	2	7 2 3
				1.4157	2	5 3 8
7	1.4184			1.4148	1	7 2 4
				1.4135	1	0 0 14
				1.3929	1	7 1 7
				1.3875	1	2 6 8
10	1.3887			1.3860	1	1 3 13
				1.3851	1	5 1 11
				1.3833	2	2 7 5
				1.3579	1	3 5 9
				1.3184	1	1 4 13
5	1.3109			1.3131	1	5 1 12
				1.3087	2	2 7 7

Data 1 = Bruker D8 Advance powder diffractometer, only down to d = 1.9351 Å; data 2 = Rigaku R-Axis Rapid II (Gandolfi-like data). The strongest diffraction maxima are shown in bold

employing JEOL and "Probe for EPMA" (Probe Software, Inc.) analysis software (wavelength-dispersive mode, 10 kV, 20 nA, 20 µm defocussed beam diameter, counting time 10 s on peak and 5 s on background positions). The following

natural reference materials and X-ray lines were used: wollastonite (Ca*K*α), kermesite (Sb*L*α, S*K*α), scorodite (As*L*α) and synthetic ZnO (Zn*L*α). If the analytical data were processed assuming an ideal formula, totals of ca. 114–117% were obtained, and the Ca, Sb and As values were all too high (especially As). If a loss of a third of all water molecules (i.e. only the hydrogen-bonded ones, see below) is assumed ("unprocessed" sum is 88%), then the total would be 101% and the Ca:Sb:As-ratio would be nearly perfect.

The calculated empirical formulae, based on O = 22 atoms per formula unit (apfu), are very similar for the two datasets: $(Ca_{0.93}Mg_{0.02})_{\Sigma 0.95}Sb_{2.02}(AsO_3)_{4.00}\cdot 10H_2O$ (Prague material) and $Ca_{1.04}Sb_{2.03}(AsO_3)_{3.92}\cdot 10H_2O$ (Vienna material). The ideal formula is $CaSb^{5+}{}_2(As^{3+}{}_2O_3)_4\cdot 10H_2O$, which we reformulated as $CaSb^{5+}{}_2O_2(As^{3+}{}_2O_5)_2\cdot 10H_2O$ to emphasise the presence of As_2O_5 dimers in the crystal structure (see below). The ideal formula requires CaO 5.87, Sb_2O_5 33.86, As_2O_3 41.41, H_2O 18.86, total 100.00 wt%.

The calculated Gladstone-Dale compatibility index ($1-K_P/K_C$; Mandarino 1981, 2007) is 0.065 (fair) using the empirical formula and single-crystal data from Vienna, and 0.071 (fair) using the empirical formula and single-crystal data from Prague. It is 0.067 using the ideal formula and the single-crystal data from Vienna. The following observation might explain the "fair" category: Prachařite contains corner-shared SbO_6 octahedra; Shannon and Fischer (2016) noticed that corner-shared octahedral network and chain structures such as perovskites, tungsten bronzes and titanite-related structures showed systematic deviations between observed and calculated polarisabilities (polarisability analysis is a more reliable measure of the compatibility of a mineral's refractive index, composition and crystal structure) and thus were excluded from their regression analysis.

Table 3 Crystal data, data collection information and refinement details for prachařite

Crystal data:	
Formula	$CaSb^{5+}{}_2(As^{3+}{}_2O_5)_2O_2\cdot 10.1H_2O$
Formula weight	957.73
Space group, *Z*	$P\bar{3}c1$ (no. 165), 6
a, *c* (Å)	13.951(2), 19.899(2)
V (Å^3)	3354.1(10)
F(000), ρ_{calc} (g·cm^{-3})	2708, 2.845
m (mm^{-1})	8.612
Absorption correction	multi-scan (Otwinowski et al. 2003)
SHELX transmission factors	0.358 (min.)–0.480 (max.)
Crystal dimensions (mm)	0.15 × 0.15 × 0.10
Data collection:	
Diffractometer	Nonius KappaCCD system
λ (Mo–*Kα*) (Å), *T* (K)	0.71073, 293
Crystal-detector distance (mm)	39
Rotation axes, width (°)	φ, ω, 1
Total number of frames	1325
Collection time per degree (s)	70
Collection mode, $2q_{max}$ (°)	full sphere, 70 (used: 64.06)
h, k, l ranges	-20 → 20, -17 → 17, -29 → 29
Total reflections measured	14,742
Unique reflections	3898 (R_{int} 2.71%)
Refinement (on F^2):	
*R*1(*F*), w*R*2$_{all}$(F^2)	2.33%, 5.75%
'Observed' reflections	3057 [$F_o > 4\sigma(F_o)$]
Extinctinction coefficient	0.00007(2)
No. of refined parameters	171
GooF	1.024
$(\Delta/\sigma)_{max}$	0.001
$\Delta\rho_{min}$, $\Delta\rho_{max}$ (e/Å^3)	-0.54, 0.83

Unit-cell parameters were refined from 9806 recorded reflections

Scattering factors for neutral atoms were employed in the refinement

X-ray crystallography

X-ray powder diffraction

Powder diffraction data were obtained using two different methods. The first data were measured in Los Angeles using a Rigaku R-Axis Rapid II curved imaging plate microdiffractometer with monochromatised Mo*K*α radiation. A Gandolfi-like motion on the φ and ω axes was used to randomise the sample. Observed *d* values and intensities were derived by profile fitting using JADE 2010 software (Materials Data, Inc.). Data (in Å for MoK_α) are given in Table 2 ("data 2"). Unit-cell parameters refined from the powder data using JADE 2010 with whole pattern fitting are: *a* = 13.952(6), *c* = 19.918(10) Å, *V* = 3358(3) Å^3.

The second data, also given in Table 2 ("data 1"), were measured using a Bruker D8 Advance powder diffractometer equipped with solid-state LynxEye detector and secondary monochromator producing Cu*K*α radiation housed at the Department of Mineralogy and Petrology, National Museum, Prague, Czech Republic. The instrument was operated at 40 kV and 40 mA. In order to minimise the background, the powder sample was placed on the surface of a flat silicon wafer in ethanol suspension. The powder pattern was collected in the Bragg–Brentano geometry in the range 3–70° 2θ, with a step size of 0.01° and a counting time of 30 s per step (the total duration of the experiment was about three days). The positions and intensities of the diffraction maxima were determined and refined using the Pearson VII profile-shape function of the ZDS program package (Ondruš 1993) and the following unit-cell parameters were refined by the least-squares program of Burnham (1962): *a* = 13.9541(5), *c* = 19.795(1) Å, *V* = 3338.0(3) Å^3.

Table 4 Fractional atomic coordinates and displacement parameters (in $Å^2$) for prachařite

Atom	*x*	*y*	*z*	U_{eq}/U_{iso}	U^{11}	U^{22}	U^{33}	U^{23}	U^{13}	U^{12}
Ca1	0.0	0.0	0.0	0.0248(2)	0.0177(3)	0.0177(3)	0.0391(7)	0.0	0.0	0.00886(15)
Ca2	2/3	1/3	0.28358(5)	0.02927(18)	0.0295(3)	0.0295(3)	0.0288(4)	0.0	0.0	0.01476(13)
Sb	0.224893(11)	0.282407(11)	-0.000062(8)	0.01942(5)	0.01592(7)	0.01518(7)	0.02593(9)	-0.00004(5)	-0.00040(5)	0.00686(5)
As1	0.16088(2)	0.488413(19)	-0.000636(14)	0.02662(7)	0.02504(12)	0.01480(11)	0.03875(16)	0.00088(9)	-0.00018(10)	0.00901(9)
As2	0.11187(2)	0.33887(2)	-0.136233(13)	0.02632(7)	0.02471(12)	0.02681(13)	0.02669(13)	0.00651(10)	0.00205(10)	0.01233(10)
O1	0.23995(13)	0.42703(13)	0.02264(9)	0.0265(4)	0.0234(8)	0.0170(7)	0.0383(10)	-0.0053(7)	-0.0054(7)	0.0094(6)
O2	0.02609(13)	0.38434(13)	0.02211(9)	0.0271(4)	0.0243(8)	0.0172(8)	0.0383(10)	-0.0027(7)	0.0023(7)	0.0094(7)
O3	0.15427(15)	0.46678(14)	-0.09049(9)	0.0314(4)	0.0325(9)	0.0231(8)	0.0391(11)	0.0078(7)	0.0025(8)	0.0143(7)
O4	-0.01605(14)	0.25575(14)	-0.09598(9)	0.0261(3)	0.0212(8)	0.0257(8)	0.0279(9)	0.0027(7)	-0.0008(7)	0.0091(7)
O5	0.20020(13)	0.29987(14)	-0.09646(9)	0.0261(3)	0.0255(8)	0.0282(8)	0.0269(9)	0.0021(7)	-0.0002(7)	0.0150(7)
O6	0.06660(12)	0.20198(13)	0.01966(8)	0.0216(3)	0.0151(7)	0.0178(7)	0.0313(9)	0.0018(6)	0.0005(6)	0.0078(6)
Ow7	0.0	0.0	0.1178(3)	0.0685(13)	0.080(2)	0.080(2)	0.046(3)	0.0	0.0	0.0398(11)
Ow8	2/3	1/3	0.16122(18)	0.0496(9)	0.0574(14)	0.0574(14)	0.0341(19)	0.0	0.0	0.0287(7)
Ow9	0.18081(19)	0.48967(18)	0.24959(13)	0.0441(5)	0.0410(12)	0.0391(11)	0.0457(13)	0.0048(10)	0.0087(10)	0.0152(10)
Ow10	0.5452(2)	0.35988(19)	0.35604(13)	0.0487(6)	0.0561(14)	0.0466(13)	0.0509(14)	0.0125(11)	0.0238(11)	0.0314(12)
Ow11	0.44436(18)	0.47501(18)	-0.14998(12)	0.0412(5)	0.0418(12)	0.0320(11)	0.0432(12)	-0.0002(10)	-0.0016(10)	0.0135(10)
Ow12	0.0993(2)	0.2890(2)	0.18037(13)	0.0587(7)	0.0453(14)	0.0789(18)	0.0507(15)	-0.0196(14)	-0.0039(12)	0.0301(13)
Ow13[a]	-0.1048(8)	0.0247(10)	0.2274(6)	0.128(6)						
H71	0.004(7)	0.051(4)	0.144(2)	0.15(2)						
H91	0.153(5)	0.465(6)	0.2087(15)	0.17(3)						
H92	0.129(2)	0.488(3)	0.2740(15)	0.058(11)						
H101	0.537(3)	0.418(2)	0.3443(17)	0.061(11)						
H102	0.500(4)	0.332(4)	0.3897(18)	0.12(2)						
H111	0.405(3)	0.414(2)	-0.127(2)	0.090(15)						
H112	0.468(3)	0.5367(19)	-0.1296(15)	0.057(11)						
H121	0.154(3)	0.285(4)	0.1585(18)	0.087(14)						
H122	0.039(2)	0.270(3)	0.1560(18)	0.069(13)						

[a]Refined occupancy of Ow13 (isotropically refined): 0.400(11); Ow13…Ow13' = 1.08(2) Å

Table 5 Selected bond distances (Å) and bond angles (°), and calculated bond-valence sums (in valence units, v.u.) for the coordination polyhedra in prachařite

Ca1–Ow7 (×2)	2.344(5)	0.344	Ca2–Ow10 (×3)	2.391(2)	0.306
–O6 (×6)	2.5176(16)	0.225	Ca2–Ow9 (×3)	2.410(2)	0.292
<Ca1–O>	2.474	2.038 v.u	Ca2–Ow8	2.435(4)	0.275
			<Ca2–O>	2.405	2.069 v.u.
Sb–O6'	1.9508(15)	0.884	As1–O1	1.7633(17)	1.028
–O6	1.9524(15)	0.881	–O2	1.7661(16)	1.021
–O1	1.9736(16)	0.842	–O3	1.8079(19)	0.925
–O2	1.9765(16)	0.837	<As1–O>	1.779	2.974 v.u.
–O4	1.9807(18)	0.830			
–O5	1.9853(18)	0.822	As2–O4	1.7611(17)	1.033
<Sb–O>	1.970	5.096 v.u	–O5	1.7641(17)	1.026
			–O3	1.8185(18)	0.902
Ow13…Ow13'	1.08(2)		<As2–O>	1.781	2.961 v.u.
As1–O3–As2	128.55(9)				
Sb–O6–Sb'	135.01(8)				

Bond-valence sums (v.u.) for O atoms O1 to Ow13 are as follows: O1 1.867; O2 1.856; O3 1.831; O4 1.865; O5 1.848; O6 1.989; Ow7 0.324; Ow8 0.280; Ow9 0.297; Ow10 0.308; Ow11 0.0; Ow12 0.0; Ow13 0.0

Hydrogen bonds

Ow7–H71···Ow13	2.741(11)	Ow11–H111···O2	2.909(3)
Ow9–H91···Ow12	2.800(4)	Ow11–H111···O5	3.222(3)
Ow9–H92···Ow11	2.828(3)	Ow11–H112···O3	2.837(3)
Ow10–H101···Ow11	2.885(3)	Ow12–H121···O4	2.858(3)
Ow10–H102···O1	2.930(3)	Ow12–H122···O5	2.930(3)

The second H atom bonded to Ow7 was not detectable. At least three possible positions were detected for H atoms bonded to Ow8; none could be refined. Ow11 and H111 are involved in a bifurcated hydrogen bond. For the partially occupied Ow13 site, two possible H sites were found but no refinement was attempted

Single-crystal X-ray diffraction

An Ewald sphere of intensity data from a fragment of a well-developed transparent prachařite crystal was collected in Vienna with a Nonius KappaCCD four-circle single-crystal diffractometer (see Table 3 for details on data collection and refinement). The crystal structure was solved and refined in space group $P\bar{3}c1$ (no. 165) using SHELX-97 (Sheldrick 2008) to $R1 = 2.3\%$ and $wR2_{all} = 5.8\%$.

An additional intensity dataset was collected in Prague using a Rigaku SuperNova single-crystal diffractometer (microfocus X-ray tube, Mo*K*a X-radiation, Atlas S2 charge-coupled device detector, 293 K, $2\theta_{max} = 59.08°$, completeness 0.98, $R_{int} = 5.1\%$). The model obtained is basically identical to the originally obtained model (albeit with standard uncertainties higher by a factor of about 1.5 to 2) and will not be discussed here except in case of notable differences. The unit-cell parameters, $a = 13.9545(4)$ Å, $c = 19.7896(5)$ Å, $V = 3337.33(16)$ Å^3, are similar except for a slightly decreased length of the c axis (a smaller c-axis length is also seen in the powder diffraction data of the corresponding material). This is tentatively attributed to variable water contents (see discussion below).

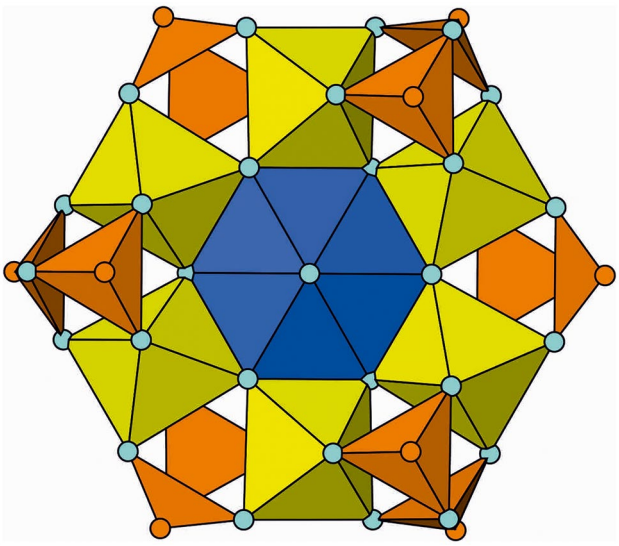

Fig. 3 The fundamental building unit in the crystal structure of prachařite: a heteropolyhedral cluster composed of corner-sharing SbO_6 octahedra (yellow), As_2O_5 dimers (with eclipsed configuration) built of AsO_3 groups (orange) and a central $Ca1O_8$ polyhedron (dark blue). Oxygen ligands are shown as small pale blue circles. Drawing done with ATOMS V. 6.3.1 (Dowty 2006)

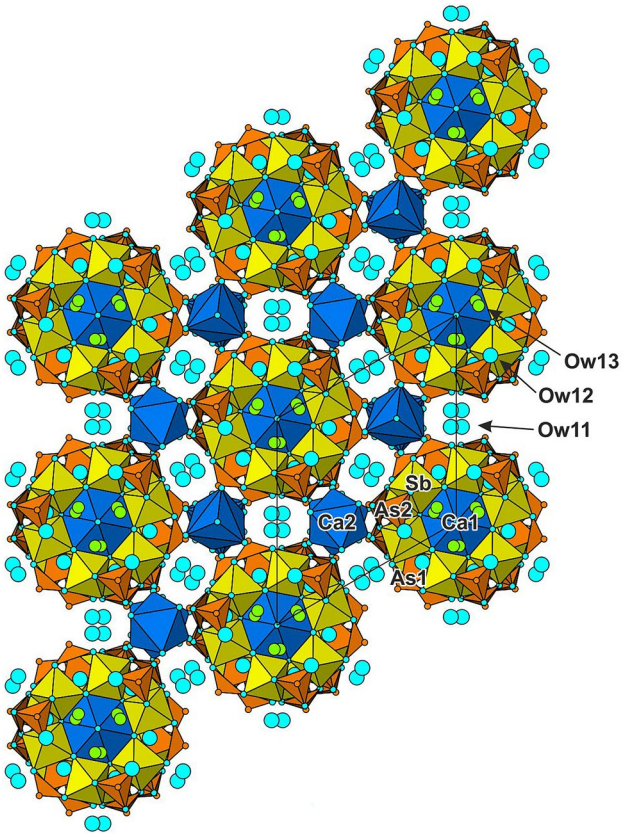

Fig. 4 The crystal structure of prachařite in a view along the *c*-axis. Ca-O polyhedra are dark blue, SbO_6 octahedra are yellow, AsO_3 groups are orange, fully occupied Ow atoms are pale blue spheres, and partly occupied Ow13 atoms are green spheres. H atoms have been omitted for clarity. The unit cell is outlined. Drawing done with ATOMS V. 6.3.1 (Dowty 2006)

Table 4 gives final atomic coordinates and displacement parameters for prachařite, while Table 5 provides selected bond lengths and angles, including calculated bond-valence sums. A CIF-file is available in the Supplement. The asymmetric unit contains two Ca, one Sb, two As, 13 O and 14 H sites, nine of which could be located and refined with the following restraints: O–H = 0.90(2) Å; H…H = 1.50(5) Å. Seven of the 13 O sites represent water molecules. One water molecule site (Ow13), located in an interlayer space, is a partially occupied split-site (occupancy ~ 0.40); the refined formula is $CaSb^{5+}{}_2(As^{3+}O_3)_4{\cdot}\sim 10.1H_2O$. The aforementioned second dataset gave a slightly decreased Ow13 occupancy, ~ 0.25, which might explain the equally slightly decreased length of the *c* axis of the fragment used for that dataset.

Prachařite has a layered structure based on two different layers (Figs. 3, 4 and 5). The first one comprises a six-membered ring of corner-sharing SbO_6 octahedra (< Sb–O > = 1.970 Å, Table 5). The eight-coordinated Ca1 atom occupies the centre of the ring (< Ca1–O > = 2.474 Å). The $Ca1O_8$ polyhedron is a hexagonal dipyramid that shares each of its horizontal edges with one of the six symmetrically equivalent SbO_6 octahedra. Thus, six ligands are O atoms (O6) and two are water molecules (Ow7). Attached to the SbO_6 octahedra by vertices are AsO_3 groups (< As1–O > = 1.779 Å, < As2–O > = 1.781 Å). The $(As1O_3)^{3-}$ and $(As2O_3)^{3-}$ groups are corner-linked to form a $(As_2O_5)^{4-}$ diarsenite group in an eclipsed configuration; thus, the structural formula was formulated as $CaSb^{5+}{}_2O_2(As^{3+}{}_2O_5)_2{\cdot}10H_2O$. The heteropolyhedral Ca-Sb-As-O-cluster represents the fundamental building unit of prachařite (Figs. 3 and 4).

The second Ca atom, Ca2, is located between two heteropolyhedral Ca1-Sb-As-O layers (Fig. 5). The Ca2 atom shows seven-fold coordination (< Ca2–O > = 2.405 Å); all ligands are water molecules (Ow10 × 3, Ow9 × 3 and Ow8). Also in the interlayer are located two fully occupied, only hydrogen-bonded water molecules, represented by Ow11 and Ow12, and the already mentioned partially occupied water molecule, Ow13 (Figs. 4 and 5). The latter is close to a symmetrically equivalent position [Ow13…Ow13' = 1.08(2) Å] and shows an increased U_{iso} value (~ 0.13 $Å^2$). Hydrogen bonds are more or less weak, with donor…acceptor distances ranging between 2.74 and 3.22 Å (Table 5). The bond-valence sums, calculated using the recently improved parameters of Gagné and Hawthorne (2015), are in very good agreement with the ideal valencies (Table 5).

Raman spectroscopy

Raman spectra (a representative one is shown in Fig. 6) were collected on a crystal lying on its (0001) face in the range 4500–10 cm^{-1} using a DXR dispersive Raman Spectrometer (Thermo Scientific) attached to an Olympus microscope. The Raman signal was excited by the green emission (532 nm) of a diode-pumped solid-state laser and analysed by a charge-coupled device detector. The experimental parameters were: 50 × objective (numerical aperture 0.50), 10 s exposure time, 100 exposures and 1 mW laser power. With a 400 lines/mm diffraction grating in the optical pathway, the spectral resolution was in the range 4.4–9.7 cm^{-1}. The spectra were repeatedly acquired from different crystals in order to obtain a representative spectrum with the best signal-to-noise ratio. A possible thermal damage of the measured spots was excluded by visual inspection of each spot after the measurement, by observation of possible decay of spectral features at the start of excitation and checking for thermal downshift of Raman lines. The instrument was set up by a software-controlled calibration procedure using multiple neon emission lines (wavelength calibration), multiple polystyrene Raman bands (laser wavelength calibration) and standardised white-light sources (intensity calibration). Spectral

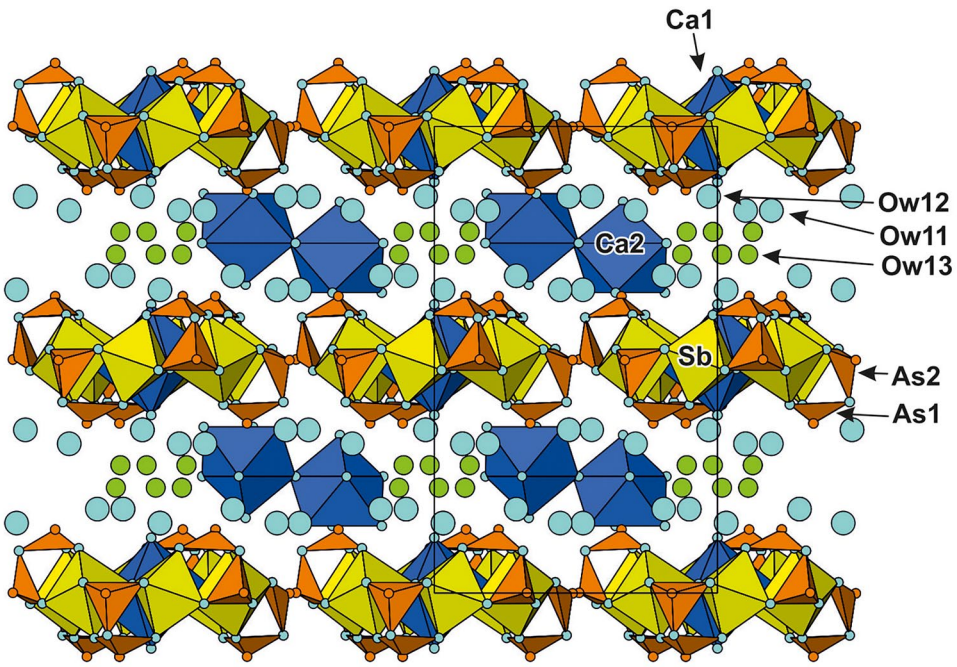

Fig. 5 The crystal structure of prachařite in a view along the *a*-axis, showing the interlayer content and the eclipsed configuration of the As_2O_5 dimer. Legend as in Fig. 4. Drawing done with ATOMS V. 6.3.1 (Dowty 2006)

manipulations were performed using the Omnic 9 software (Thermo Scientific). The lateral resolution was ~ 0.7 µm in confocal mode.

The main bands observed are (in cm^{-1}, strong bands underlined): 3620, 3470, 3383, 3288, 1655, 851, 840, 830, 792, 541, 458, 358, 297, 273, 253, 233, 185, 129, 116, 63 and 24. The dominant bands in the 600–200 cm^{-1} region can be assigned to δ As–O–As and AsO_2 vibrations of the $(As_2O_5)^{4-}$ diarsenite group (see above description of crystal structure). Weaker bands in the range 900–750 cm^{-1} may be related to stretching (symmetric and antisymmetric) vibrations of As–O bonds, as well as to Sb–O vibrations of the SbO_6 octahedron (Vandenborre et al. 1980; Baran and Botto 1981; Devi and Vidyasagar 1998; Castro et al. 2009; Bahfenne and Frost 2010; Glamazda et al. 2017). The bands in the 200–10 cm^{-1} region are caused by lattice modes. The presence of water is documented by a broad

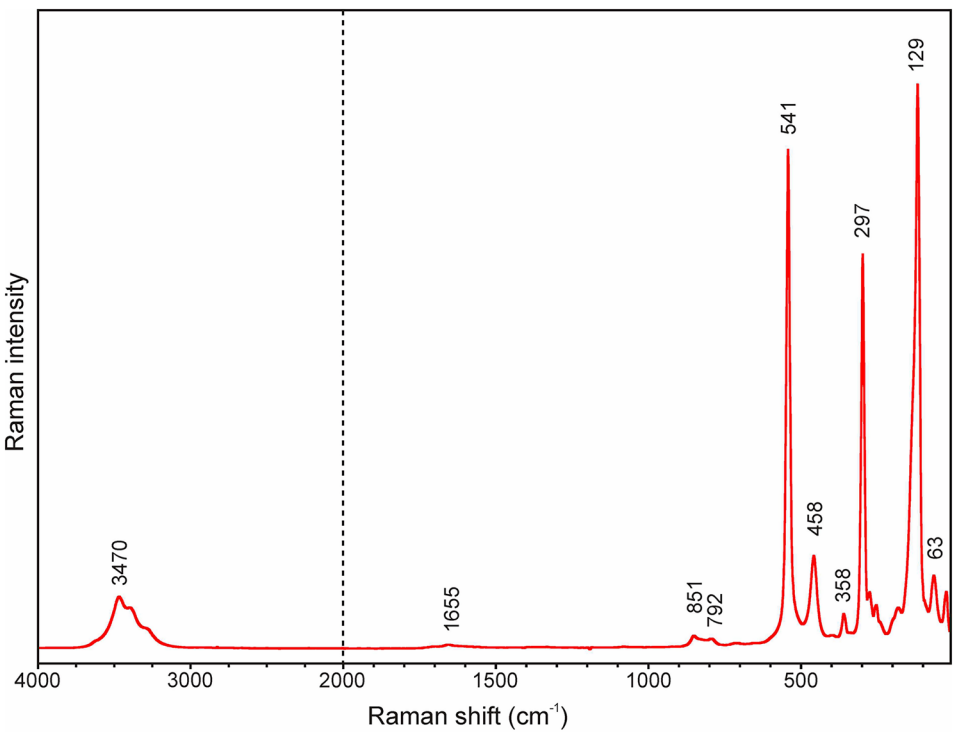

Fig. 6 Raman spectrum of prachařite (split at 2000 cm^{-1})

OH-stretching band running from 3800 to 3100 cm^{-1} with recognisable components at 3620, 3470, 3383 and 3288 cm^{-1}; at least four distinct components in this area indicate several structurally non-equivalent water molecules, in agreement with the crystal-structure determination. Following the correlation curve of Libowitzky (1999), the band component at 3288 cm^{-1} probably corresponds to the hydrogen bond Ow7–H71···Ow13 [2.741(11) Å] (Table 5), while the 3470 and 3383 cm^{-1} components would correspond to at least five different H bonds with O···O distances between 2.80 and 2.89 Å. The band component at 3620 cm^{-1} is probably related to the very weak hydrogen bond Ow11–H111···O5. A weak band at 1655 cm^{-1} is assigned to the ν_2 (δ) bending vibrations of water molecules.

Discussion

Relation to other mineral species

No close relationship with other minerals is apparent. Specifically, there is neither a known mineral species nor a known synthetic compound that both contains Sb^{5+} and As^{3+}. Interestingly, whitecapsite, $H_{16}Fe_5^{2+}Fe_{14}^{3+}Sb_6^{3+}(AsO_4)_{18}O_{16}{\cdot}120H_2O$ (Pekov et al. 2014) contains both Sb^{3+} and As^{5+}; its structure is based on a complex heteropolyhedral $[(\square,Fe^{2+})_6Fe^{3+}_7Sb_3O_8(AsO_4)_9(H_2O)_{30}]$ (□ = vacancy) cluster. Smamite, triclinic $Ca_2Sb(OH)_4[H(AsO_4)_2]{\cdot}6H_2O$ (Plášil et al. 2020), also contains both Sb^{3+} and As^{5+}. Its atomic arrangement is based upon $\{Ca_2(H_2O)_6Sb(OH)_4[H(AsO_4)_2]\}$ infinite chains consisting of edge-sharing dimers of $Ca(H_2O)_3O_2(OH)_2$ polyhedra which share edges with $Sb(OH)_4O_2$ octahedra. A recently described mineral containing both Sb^{3+} and As^{3+} is lepageite, $Mn^{2+}_3(Fe^{3+}_7Fe^{2+}_4)O_3[Sb^{3+}_5As^{3+}_8O_{34}]$ (Pieczka et al. 2019), which was found in the Szklary pegmatite (Lower Silesia, Poland). Seven other minerals are presently known to contain diarsenite groups (listed in chronological order of published crystal-structure determination): paulmooreite, $Pb_2As_2O_5$; gebhardite, $Pb_8(As_2O_5)_2OCl_6$; fetiasite, $(Fe^{3+},Fe^{2+},Ti)_3(As_2O_5)O_2$; vajdakite, $[(Mo^{6+}O_2)_2(H_2O)_2As^{3+}_2O_5]{\cdot}3H_2O$; schneiderhöhnite, $Fe^{2+}Fe^{3+}_3As^{3+}_5O_{13}$; karibibite, $Fe^{3+}_3(As^{3+}O_2)_4(As^{3+}_2O_5)(OH)$; and bianchiniite, $Ba_2(TiV)(As_2O_5)_2OF$. Among these, vajdakite is the only other hydrated phase.

We are not aware of the presence of any other isolated SbO_6-based Sb_6O_{30} rings in either minerals or synthetic compounds. Although rings of edge-sharing SbO_6 octahedra exist in rosiaite, $PbSb_2O_6$ (Basso et al. 1996), and isotypic compounds, they share edges with neighbouring rings to form an interrupted gibbsite-like layer.

Stability and occurrence

Prachařite has formed by weathering of a hydrothermal As-Sb-Pb–Zn(-Ag) ore vein in an estimated temperature range of 10–18 °C (based on long-term observations of the underground microclimate during different seasons) and under slightly acidic and slightly oxidising conditions. The E_h (redox potential) range must be fairly narrow since Sb^{5+} and As^{3+} must be simultaneously (meta-?)stable. Although thermodynamically, a mineral containing both Sb^{5+} and As^{3+} should not be stable, in reality, this is considered very possible because the stability boundaries Sb^{3+}/Sb^{5+} and As^{3+}/As^{5+} are very close and other arsenite minerals exist that should not be thermodynamically stable, e.g. tooeleite, $Fe^{3+}_6(As^{3+}O_3)_4(SO_4)(OH)_4{\cdot}4H_2O$ (Juraj Majzlan, pers. comm. to U.K.). Furthermore, it was reported that in a relatively reducing sediment impacted by As- and Sb-rich mining waste, most of the As is reduced to As^{3+}, while Sb^{5+} bound to the oxygen phase persists and represents 58% of the total Sb (Fawcett and Jamieson 2011). Other researchers made similar observations (Mitsunobu et al. 2006; Ritchie et al. 2013; Fawcett et al. 2015). Conditions that would favour the crystallisation of prachařite are assumed to occur also in geologically similar deposits such as the Sainte-Marie-aux-Mines ore district, Haut-Rhin department, France (von Eller and Weil 1966; Fluck 1968), which is, as mentioned above, the type locality of the chemically similar mineral smamite, $Ca_2Sb(OH)_4[H(AsO_4)_2]{\cdot}6H_2O$, the latter also occuring on one of the studied prachařite specimens.

Supplementary Information The online version contains supplementary material available at https://doi.org/10.1007/s00710-023-00830-5.

Acknowledgements Constructive comments by two anonymous reviewers and Guest Editor Karen Friese helped to improve the manuscript. The study was financially supported by the Ministry of Culture of the Czech Republic (long-term project DKRVO 2019-2023/1.II.e; National Museum, 00023272, to JS).

Open Access This article is licensed under a Creative Commons Attribution 4.0 International License, which permits use, sharing, adaptation, distribution and reproduction in any medium or format, as long as you give appropriate credit to the original author(s) and the source, provide a link to the Creative Commons licence, and indicate if changes were made. The images or other third party material in this article are included in the article's Creative Commons licence, unless indicated otherwise in a credit line to the material. If material is not included in the article's Creative Commons licence and your intended use is not permitted by statutory regulation or exceeds the permitted use, you will need to obtain permission directly from the copyright holder. To view a copy of this licence, visit http://creativecommons.org/licenses/by/4.0/.

References

Bahfenne S, Frost R (2010) A review of the vibrational spectroscopic studies of arsenite, antimonite, and antimonate minerals. Appl Spectrosc Rev 45:101–129

Baran EJ, Botto IL (1981) Vibrational spectra of $NaSbO_3$. An Asoc Quim Argent 69:283–291 (in Spanish)

Basso R, Lucchetti G, Zefiro L, Palenzona A (1996) Rosiaite, $PbSb_2O_6$, a new mineral from the Cetine mine, Siena, Italy. Eur J Mineral 8:487–492

Bonsall TA, Spry PG, Voudouris PCh, Tombros S, Seymour KS, Melfos V (2011) The geochemistry of carbonate-replacement Pb-Zn-Ag mineralization in the Lavrion district, Attica, Greece: fluid inclusion, stable isotope, and rare earth element studies. Econ Geol 106:619–651

Burnham CW (1962) Lattice constant refinement. Carnegie Inst Wash Year 61:132–135

Castro MC Jr, Carvalho EFV, Paraguassu W, Ayala AP, Snyder FC, Lufaso MW, de Araujo PCW (2009) Temperature-dependent Raman spectra of Ba_2BiSbO_6 ceramics. J Raman Spectrosc 40:1205–1210

Devi RN, Vidyasagar K (1998) Synthesis and characterization of new vanadates of antimony, $ASbV_2O_8$ (A = K, Rb, Tl or Cs). J Chem Soc, Dalton Trans 1998:3013–3020

Dowty E (2006) ATOMS V6.3.1 for atomic-structure display. Shape Software, 521 Hidden Valley Road, Kingsport, TN 37663 USA

Fawcett SE, Jamieson HE (2011) The distinction between ore processing and post-depositional transformation on the speciation of arsenic and antimony in mine waste and sediment. Chem Geol 283:109–118

Fawcett SE, Jamieson HE, Nordstrom DK, McCleskey RB (2015) Arsenic and antimony geochemistry of mine wastes, associated waters and sediments at the Giant Mine, Yellowknife, Northwest Territories. Canada Appl Geochem 62:3–17

Fluck F (1968) Description et minéralogie des mines de la région de Sainte-Marie-aux-Mines (Haut-Rhin). Bull Serv Carte Géol Als Lorr 21(2):63–120 (in French)

Frenzel M, Voudouris P, Cook NJ, Ciobanu CL, Gilbert S, Wade B (2022) Evolution of a large hydrothermal ore-forming system recorded by sulphide mineral chemistry: A case study from the Plaka Pb-Zn-Ag Deposit, Lavrion, Greece. Miner Deposita 57:417–438

Gagné OC, Hawthorne FC (2015) Comprehensive derivation of bond-valence parameters for ion pairs involving oxygen. Acta Crystallogr B 71:562–578

Glamazda A, Lemmens P, Do S-H, Choi K-Y (2017) Comparative Raman scattering study of $Ba_3MSb_2O_9$ (M = Zn, Co and Cu). Low Temp Phys 43:543–550

Kolitsch U, Rieck B, Brandstätter F, Schreiber F, Fabritz KH, Blaß G, Gröbner J (2014) Neufunde aus dem altem Bergbau und den Schlacken von Lavrion (I). Mineralien-Welt 25(1):60–75

Leleu M (1966) Les gisements plombo-zincifères du Laurium (Grèce). Sci De La Terre XI(3):293–343 (in French)

Leleu M (1969) Pseudovein mineralization and its formation medium: vein 80 (Laurium, Greece). Bull Soc Fr Minéral Cristallogr 92:101–104 (in French)

Libowitzky E (1999) Correlation of O-H stretching frequencies and O-H···O hydrogen bond lengths in minerals. Monatsh Chem 130:1047–1059

Mandarino JA (1981) The Gladstone-Dale relationship: Part IV. The compatibility concept and its application. Can Mineral 19:441–450

Mandarino JA (2007) The Gladstone-Dale compatibility of minerals and its use in selecting mineral species for further study. Can Mineral 45:1307–1324

Mitsunobu S, Harada T, Takashi Y (2006) Comparison of antimony behavior with that of arsenic under various soil redox conditions. Env Sci Technol 40:7270–7276

Ondruš P (1993) A computer program for analysis of X-ray powder diffraction patterns. Mat Sci Forum, EPDIC-2. Enchede 133–136:297–300

Otwinowski Z, Borek D, Majewski W, Minor W (2003) Multiparametric scaling of diffraction intensities. Acta Crystallogr A 59:228–234

Pieczka A, Cooper MA, Hawthorne FC (2019) Lepageite, $Mn^{2+}{}_3(Fe^{3+}{}_7Fe^{2+}{}_4)O_3[Sb^{3+}{}_5As^{3+}{}_8O_{34}]$, a new arsenite-antimonite mineral from the Szklary pegmatite, Lower Silesia, Poland. Am Mineral 104:1043–1050

Plášil J, Kampf AR, Meisser N, Lheur C, Brunsperger T, Škoda R (2020) Smamite, $Ca_2Sb(OH)_4[H(AsO_4)_2]\cdot 6H_2O$, a new mineral and a possible sink for Sb during weathering of fahlore. Am Mineral 105:555–560

Pekov IV, Zubkova NV, Göttlicher J, Yapaskurt VO, Chukanov NV, Lykova IS, Belakovskiy DI, Jensen MC, Leising JF, Nikischer AJ, Pushcharovsky DY (2014) Whitecapsite, a new hydrous iron and trivalent antimony arsenate mineral from the White Caps mine, Nevada, USA. Eur J Mineral 26:577–587

Pouchou JL, Pichoir F (1985) "PAP" (πρZ) procedure for improved quantitative microanalysis. In: Analysis M (ed) Armstrong JT. San Francisco Press, California, pp 104–106

Rieck B, Rieck P (1999) Silber, Arsen und Antimon: Vererzungen im Revier Plaka (Teil 2). Lapis 24(7–8):59–60

Rieck B, Kolitsch U, Voudouris P, Giester G, Tzeferis P (2018) Weitere Neufunde aus Lavrion, Griechenland. Mineralien-Welt 29(5):32–77

Rieck B, Kolitsch U, Voudouris P, Giester G, Tzeferis P (2020) Lavrion, Griechenland: Weitere Neufunde aus dem berühmten Bergbaurevier. Mineralien-Welt 31(3):6–21

Rieck B, Kolitsch U, Voudouris P, Giester G, Tzeferis P (2022) Neubestimmungen aus dem Minenbezirk Lavrion, Griechenland. Mineralien-Welt 33(5):6–20

Ritchie VJ, Ilgen AG, Mueller SH, Trainor TP, Goldfarb RJ (2013) Mobility and chemical fate of antimony and arsenic in historic mining environments of the Kantishna Hills district, Denali National Park and Preserve, Alaska. Chem Geol 335:172–188

Scheffer C, Tarantola A, Vanderhaeghe O, Voudouris P, Spry PG, Rigaudier T, Photiades A (2019) The Lavrion Pb-Zn-Ag–rich vein and breccia detachment-related deposits (Greece): Involvement of evaporated seawater and meteoric fluids during postorogenic exhumation. Econ Geol 114:1415–1442

Shannon RD, Fischer RX (2016) Empirical electronic polarizabilities of ions for the prediction and interpretation of refractive indices. I.Oxides and oxysalts. Am Mineral 101:2288–2300

Sheldrick GM (2008) A short history of *SHELX*. Acta Crystallogr A 64:112–122

Skarpelis N (2007) The Lavrion deposit (SE Attica, Greece): geology, mineralogy and minor elements chemistry. N Jahrb Mineral, Abh 183:227–249

Skarpelis N, Argyraki A (2009) Geology and origin of supergene ores in Lavrion (Attica, Greece). Resour Geol 59:1–14

Vandenborre MT, Husson E, Brusset H, Cerez A (1980) Spectres de vibration et calcul du champ de force des antimoniates de structure 'type $PbSb_2O_6$.' Spectrochim Acta, Part A 36:1045–1052 (in French)

von Eller J-P, Weil R (1966) Les gîtes métallifères de la région de Sainte-Marie-aux-Mines (Haut-Rhin). Bull Serv Carte Géol Als Lorr 15(2):69–80 (in French)

Voudouris P, Melfos V, Spry PG, Bonsall T, Tarkian M, Economou-Eliopoulos M (2008) Mineralogical and fluid inclusion constraints on the evolution of the Plaka intrusion-related ore system, Lavrion, Greece. Mineral Petrol 93:79–110

Wendel W, Markl G (1996) Eine Antimonit-Paragenese und weitere Neufunde aus Lavrion. Lapis 21(11):40–42, 62

Publisher's Note Springer Nature remains neutral with regard to jurisdictional claims in published maps and institutional affiliations.